Computational Electrochemistry. Simulations of Homogeneous Chemical Reactions in the Confluence Reactor and Channel Flow Cell

Nicholas P. C. Stevens[†]

Chemistry Department, Trent University, 16600 West Bank Drive, Peterborough, Ontario, Canada, K9J 7B8

Kerry A. Gooch and Adrian C. Fisher*

School of Chemistry, University of Bath, Claverton Down, Bath, BA2 7AY, U. K.

Received: June 23, 1999; In Final Form: October 18, 1999

The finite element method (FEM) is employed to simulate steady-state convection diffusion problems involving electrode processes and coupled homogeneous kinetic reactions in the channel cell and the confluence reactor. Initial FEM simulations are reported for EC, ECE, and DISP reactions in the channel cell, and the results are shown to agree with previous art. Calculations reveal the FEM extends the kinetic range accessible for such mechanisms beyond those reported previously using the backward implicit finite difference method. The FEM is then applied to simulate, for the first time, the quantitative effects of coupled homogeneous reactivity on the voltammetric response of the confluence reactor. Specifically, a working surface is presented for the application of the confluence reactor to the investigation of the CE type reactions. This surface provides a quantitative relationship between the chemical reaction rate, volume flow rate, and inlet concentrations using this new device. In all simulations performed, the FEM is found to be a highly efficient and accurate alternative to the finite difference method when applied to hydrodynamic voltammetric measurements.

Introduction

The study of homogeneous chemical kinetics using hydrodynamic devices is now well established in electrochemistry and analytical science.[1−11] A number of these techniques, including the channel flow cell,[12] (Figure 1) have been employed with great success to study the mechanisms and rates of complex electrochemical processes. The quantitative mechanistic and kinetic elucidation is typically performed using either an analytical and semiempirical or numerical simulation strategy.

The increasing complexity of the systems under investigation has required the development of new devices and more powerful strategies for the quantitative analysis of the processes occurring. Recently, we have presented some alternative experimental[13] and numerical methods[14] that offer potential benefits over previous approaches. Numerically, we have employed the FEM to solve the fluid dynamics and convection−diffusion problems associated with a new experimental device termed the confluence reactor (Figure 2). This permits the well-defined mixing of two separate reagent streams in a predefined reactor chamber.

Up to now, our FEM numerical analysis has not encompassed the inclusion of coupled chemical reactivity or multiple chemical species in the system equations. In this article, we address this specific issue and present numerical simulations that include chemical reactivity for the channel flow cell and the confluence reactor. In the case of the channel flow cell, EC, ECE, and DISP processes (detailed below) have been well-characterized previously, and the FEM is shown to be capable of reproducing the analytical and numerically reported results, using only modest computational resources. The particular suitability of the FEM technique to simulations where the rate constants are extremely large, up to levels where the rate of diffusion becomes limiting, is demonstrated.

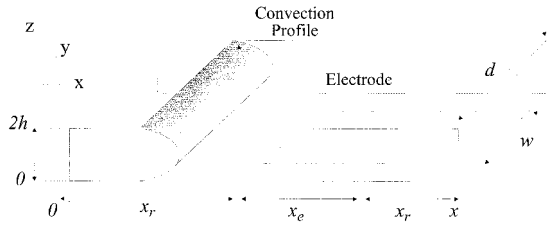

Figure 1. Schematic of channel cell.

The ECE and DISP reactions are characterized by the apparent transfer of more than one electron to each reactant molecule, resulting from the further reaction of the initial product A to form a species C, which then accepts another electron. This second electron may come from the electrode in the ECE mechanism, shown in step 3 below, or from the DISP (disproportionation) reaction, shown in step 4 below.

$$\text{Step 1: } A + e^- \rightarrow B$$

$$\text{Step 2: } B \rightarrow C \qquad \text{rate constant } k_2$$

$$\text{Step 3: } C + e^- \rightarrow D$$

$$\text{Step 4: } B + C \rightarrow A + D \qquad \text{rate constant } k_4$$

We will adopt Compton's notation[1] of k_n and k_{-n} for the forward and backward rate constants of reaction *n*. In the DISP mechanism, the rate-determining step may be either step 2 (DISP1) or 4 (DISP2). In both cases, steps 2−4 may be approximated as 2B → A + D, but with a first-order rate constant of k_2 for the DISP1 mechanism or a second-order rate constant of k_2k_4/k_{-2} for the DISP2 case.

[†] E-mail: nstevens@trentu.ca.

* A.C.Fisher@bath.ac.uk. Telephone: 44 1225 826 627. Fax: 44 1225 826 231.

10.1021/jp992091w CCC: $19.00
Published on Web 01/22/2000

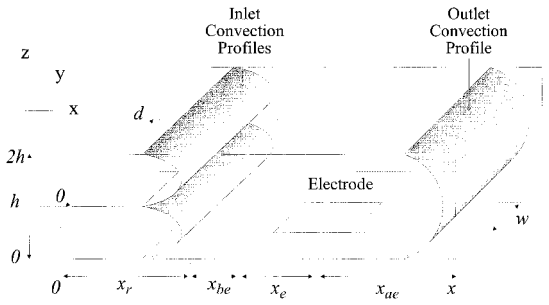

Figure 2. Schematic of confluence reactor.

Compton et al. revealed the ability of the channel electrode geometry to distinguish between the ECE and DISP reactions by examining the flow rate dependence of the transport limited current. As the flow rate is increased relative to the rate of reaction, the intermediate species B and C are removed from the vicinity of the electrode, and n_{eff},

$$\frac{\text{total current}}{\text{current for A} \rightarrow \text{B}}$$

the apparent number of electrons transferred falls from the upper limit of 2 to the lower limit of 1. Previous investigations have shown how working curves can be constructed for the factor n_{eff} for channel cell geometry, and these are reproduced using the FEM.

The EC mechanism is described by steps 1 and 2 above, where step 2 is irreversible. The number of electrons transferred at the limit is therefore always one, but the depletion of B at the electrode caused by the subsequent reaction shifts the potential required for the reduction of A to B toward more positive potentials. This is commonly described by measuring the half-wave potential, the potential at which the current is equal to half of the transport limited current. This characterization is appropriate, as the shape of the overall wave does not vary with the rate of the reaction.

For the confluence reactor, FEM modeling is applied to establish the response of the device to systems undergoing CE reactions. The reaction scheme may be stated as follows.

$$\text{Step 1: A} + \text{B} \rightarrow \text{C} \quad \text{rate constant } k_{\text{CE}}$$

$$\text{Step 2: C} + \text{e}^- \rightarrow \text{D}$$

This particular mechanism is difficult to probe using standard hydrodynamic techniques, due to the reactions occurring as the reagents are mixed. A unique working surface is demonstrated relating the results where kinetic processes occur to the responses in the absence of such kinetics. To model the CE reaction, two different species are introduced into the confluence reactor through the separate inlets. These mix and react at some point after the union of the inlets, producing an electroactive species C, which is reduced at an electrode placed downstream of the union of the inlets. In all the simulations, the FEM is shown to be a powerful and efficient alternative to the previously employed finite difference method.

Theory

Grid Formation. For channel flow cell simulations, a cell of the form shown in Figure 1 is employed. The concentration profile over the electrode region is essentially two-dimensional in form provided that the electrode is cited centrally within the duct and is substantially smaller than the duct width. A similar argument holds for the confluence reactor. The region of interest may therefore be discretised into triangular elements as shown in Figure 3. The grids chosen are highly nonuniform, with the elements near the electrode being typically over 4 orders of magnitude smaller than those furthest away, forming a geometric series as previously described.[15] The grid parameters of the simulations are shown on the figures, with those of the type *x* or *z* denoting the size of the grid over the regions shown, and the size of the smallest elements in each direction denoted by the same variables with an extra *f* subscript. The number of elements over each region is given by those parameters of the form n_{sub} where the subscript indicates the region.

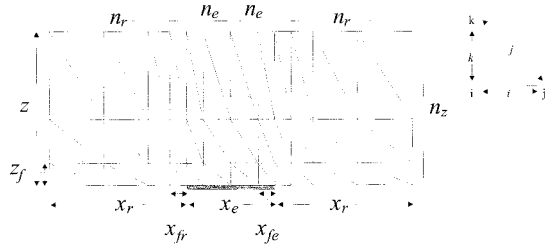

Figure 3. Discretisation of channel cell into grid of triangular elements.

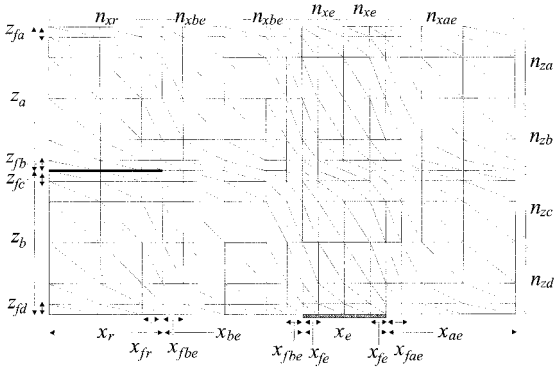

Figure 4. Discretisation of confluence reactor into grid of triangular elements.

The confluence reactor may be discretised into a mesh of triangles as shown in Figure 4.

Hydrodynamic Simulation. The convective profiles for the confluence reactor are more complex than the parabolic flow in the channel cell and are found by the solution of the Navier–Stokes equations, also using a finite element method. These equations are

$$\nu\left(\frac{\partial^2 u}{\partial x^2} + \frac{\partial^2 u}{\partial z^2}\right) - \frac{1}{\rho}\frac{\partial p}{\partial x} - u\frac{\partial u}{\partial x} - w\frac{\partial u}{\partial z} = 0 \qquad (1)$$

$$\nu\left(\frac{\partial^2 w}{\partial x^2} + \frac{\partial^2 w}{\partial z^2}\right) - \frac{1}{\rho}\frac{\partial p}{\partial x} - u\frac{\partial w}{\partial x} - w\frac{\partial w}{\partial z} = 0 \qquad (2)$$

$$\frac{\partial u}{\partial x} + \frac{\partial w}{\partial z} = 0 \qquad (3)$$

where the kinematic viscosity, ν is given by μ/ρ, where μ is the viscosity, ρ is the density of the solution, and u and w are the velocities in the x and z directions, respectively. These equations are solved over a two-dimensional grid similar to that used for the diffusional simulations, with boundary conditions and matrix formation as previously discussed. The matrix

formation and solution of these equations has also been widely investigated in the literature.[16,17]

Matrix Formation. The general form of the equation governs the flux of any species through the two-dimensional region shown, where diffusive and convective transport operate, and there are sources and sinks where the species is generated or decays are given by

$$\frac{\partial C}{\partial t} = D\frac{\partial^2 C}{\partial x^2} + D\frac{\partial^2 C}{\partial z^2} - u\frac{\partial C}{\partial x} - w\frac{\partial C}{\partial z} - k_d C - k_s \quad (4)$$

where C is the concentration of the species and k_s and k_d are the rates of generation and decay, respectively, of the species at the point in question. For the channel electrode, the fully developed flow in the central region of the channel follows the analytical relation

$$u = u_0(1 - (h - z)^2/h^2) \quad (5)$$

where u is the velocity in the x direction, h is the half-height of the cell, and u_0 is the center velocity. It should be noted that the sources for each species are dependent on the local concentrations only of other species and are independent of the local concentration of the species in question, but that the rates of decay of the species concerned are always functions of their local concentration. If the rate of decay of a species is a higher order function of the local concentration, then an iterative method must be employed, in which the first-order rate of reaction is approximated as $k_{eff} = k_d C^x$ where C^x, is the local concentration at the previous iteration, raised to the necessary power. The iterative routine then repeats until a sufficiently small change in the concentration profile is found.

The variation of the concentration of each species is described within each element as the sum of the interpolation functions at each node, multiplied by the nodal concentrations.

$$C(x,y) = N_i(x,z)C_i + N_j(x,z)C_j + N_k(x,z)C_k \quad (6)$$

The interpolation function of a node is defined to be unity at that node, and zero at all other nodes and can therefore be derived from the nodal coordinates as

$$N_n(x,z) = (a_n + b_n x + c_n z)/2A \quad (7)$$

where n is the node concerned, $a_i = x_j z_k - x_k z_j$, $a_j = x_k z_i - x_i z_k$, $a_k = x_i z_j - x_j z_i$, $b_i = z_j - z_k$, $b_i = z_k - z_i$, $b_k = z_i - z_j$, $c_i = x_k - x_j$, $c_j = x_i - x_k$, and $c_k = x_j - x_i$, where x and z are the coordinates of the nodes of the element and A is the area of the element.

By substituting eq 6 into the governing equations for the system, a function of the concentration profile may be transformed into a matrix equation of the form

$$[K]\vec{C} = [P] \quad (8)$$

where the matrix [K] and vector [P] are derived from the nodal coordinates and other constants in the governing equations and $\vec{C}$ is the vector of the nodal concentrations. This is then solved by a standard Gaussian scheme, using a banded storage method to reduce the computational requirements.

The finite element form of eq 4 for a triangular element using the linear interpolation function described above is therefore

$$\frac{D}{4A^{(e)}}\begin{bmatrix} b_i^2 + c_i^2 & b_ib_j + c_ic_j & b_ib_k + c_ic_k \\ b_ib_j + c_ic_j & b_j^2 + c_j^2 & b_jb_k + c_jc_k \\ b_ib_k + c_ic_k & b_jb_k + c_jc_k & b_k^2 + c_k^2 \end{bmatrix} - \frac{u}{6}\begin{bmatrix} b_i & b_j & b_k \\ b_i & b_j & b_k \\ b_i & b_j & b_k \end{bmatrix} - \frac{w}{6}\begin{bmatrix} b_i & b_j & b_k \\ b_i & b_j & b_k \\ b_i & b_j & b_k \end{bmatrix} - \frac{k_d A^{(e)}}{12}\begin{bmatrix} 2 & 1 & 1 \\ 1 & 2 & 1 \\ 1 & 1 & 2 \end{bmatrix} = \frac{k_{si} l_i}{2}\begin{bmatrix} 1 \\ 1 \\ 0 \end{bmatrix} + \frac{k_{sj} l_j}{2}\begin{bmatrix} 0 \\ 1 \\ 1 \end{bmatrix} + \frac{k_{sk} l_k}{2}\begin{bmatrix} 1 \\ 0 \\ 1 \end{bmatrix} + \frac{k_s A^{(e)}}{3}\begin{bmatrix} 1 \\ 1 \\ 1 \end{bmatrix} \quad (9)$$

where k_s is subdivided up into k_i, k_j, and k_k for sources that operate on only the boundaries of element on the sides indicated, as shown in Figure 2, and k_s for sources over a whole element.

The general equation and finite element matrix equation governing the transport of material through the confluence reactor are identical to those for the channel cell, given by eqs 4 and 9.

EC Reaction. For the EC reaction, the exact equations governing the system are

$$D\frac{\partial^2 C_A}{\partial x^2} + D\frac{\partial^2 C_A}{\partial z^2} - u\frac{\partial C_A}{\partial x} = 0 \quad (10)$$

$$D\frac{\partial^2 C_B}{\partial x^2} + D\frac{\partial^2 C_B}{\partial z^2} - u\frac{\partial C_B}{\partial x} - k_2 C_B = 0 \quad (11)$$

$$D\frac{\partial^2 C_C}{\partial x^2} + D\frac{\partial^2 C_C}{\partial z^2} - u\frac{\partial C_C}{\partial x} - k_2 C_B = 0 \quad (12)$$

with the boundary conditions

$z = 0$	$x < x_r$	$dC_A/dz = 0$	$dC_B/dz = 0$	$dC_C/dz = 0$
$z = 0$	$x_r < x < x_r + x_e$	$C_A = \exp\theta\, C_B$	$dC_B/dz = -dC_A/dz$	$dC_C/dz = 0$
$z = 0$	$x_r + x_e < x$	$dC_A/dz = 0$	$dC_B/dz = 0$	$dC_C/dz = 0$
$z = 2h$	all x	$dC_A/dz = 0$	$dC_B/dz = 0$	$dC_C/dz = 0$
all z	$x = 0$	$C_A = C_{A\,bulk}$	$C_B = 0$	$C_C = 0$
all z	$x = 2x_r + x_e$	$dC_A/dx = 0$	$dC_B/dx = 0$	$dC_C/dx = 0$

where $\theta = (F/RT)(E - E_0)$ and C_X is the concentration of species X. The rate constant k_2 appears as a decay term of the form k_d in eq 11 but as a source term of the form k_s in eq 12. The gradient boundary condition for species B at the electrode is expressed in the form of a k_{s1} contribution to the right-hand side vector. The interdependence of the boundary conditions at the electrode surface requires an iterative scheme to be employed to solve the equations. The initial values chosen for the concentrations at the electrode for species A and B were found as $C_A = (1 + (k_2 + 1)e^{-\theta})^{-1}$ and $C_B = (1 + e^{\theta} + k_2)^{-1}$, proceeding from the assumptions that $C_A + C_B + C_C = 1$, $C_B/C_C = k_2$, and $C_A/C_B = e^{-\theta}$. This estimate was found to give a good initial approximation to the final answer. An iterative procedure was then followed to relax these initial estimates to the true solution. This entailed calculating the distribution of A, using the values of the concentration of B from the previous iteration, and calculating a new distribution of B using those values for A. The values of B used in the next iteration are then set by the formula

$$C_B = (1 - re)C_{B0} + reC_{B1} \quad (13)$$

where re is a relaxation constant normally varying between 0.4 and 0.02, C_{B0} is the value carried forward from the last iteration,

and C_{B1} is the value just calculated. This is repeated until the largest change at any point, measured as ch $= |C_{B0}/C_{B1}| - 1$, fell below a set tolerance, normally 1×10^{-3} to 1×10^{-5}, depending on the level of complexity of the simulation. Only points at which C_{B1} was at least $5 \times 10^{-4} C_{bulk}$ were considered in this check, below which level numerical noise becomes evident. The value of re was also progressively decreased as the value of ch fell, normally halving for every decade past 0.01, which was found to bring the simulation to convergence smoothly.

To further minimize computational requirements in the iterative schemes employed, where a potential or rate constant was sequentially increased, the converged concentration distribution found for each run was used as the initial distribution for the next.

To predict the current response for the EC reaction, it is only necessary to consider species A and B. As species C is not electroactive, it does not affect the observed steady-state response in any way, and it may be calculated after converged values of A and B are found.

ECE Reaction. The ECE reaction is similar to the EC reaction defined above for species A and B, with the further contribution that species C is itself electroactive. The fact that n_{eff} varies with flow rate has led to this reaction normally being studied at potentials sufficient to cause complete conversion of A to B at the electrode. If the reduction potential for C is sufficiently negative of the reduction potential of A then C may also be considered to be converted completely to D. The governing equations are therefore

$$D\frac{\partial^2 C_A}{\partial x^2} + D\frac{\partial^2 C_A}{\partial z^2} - u\frac{\partial C_A}{\partial x} = 0 \quad (14)$$

$$D\frac{\partial^2 C_B}{\partial x^2} + D\frac{\partial^2 C_B}{\partial z^2} - u\frac{\partial C_B}{\partial x} - k_2 C_B = 0 \quad (15)$$

$$D\frac{\partial^2 C_C}{\partial x^2} + D\frac{\partial^2 C_C}{\partial z^2} - u\frac{\partial C_C}{\partial x} - k_2 C_B = 0 \quad (16)$$

$$D\frac{\partial^2 C_D}{\partial x^2} + D\frac{\partial^2 C_D}{\partial z^2} - u\frac{\partial C_D}{\partial x} = 0 \quad (17)$$

with the boundary conditions

$z = 0$	$x < x_r$	$dC_A/dz = 0$	$dC_B/dz = 0$	$dC_C/dz = 0$	$dC_D/dz = 0$
$z = 0$	$x_r < x < x_r + x_e$	$C_A = 0$	$dC_B/dz = -dC_A/dz$	$C_C = 0$	$dC_D/dz = -dC_C/dz$
$z = 0$	$x_r + x_e < x$	$dC_A/dz = 0$	$dC_B/dz = 0$	$dC_C/dz = 0$	$dC_D/dz = 0$
$z = 2h$	all x	$dC_A/dz = 0$	$dC_B/dz = 0$	$dC_C/dz = 0$	$dC_D/dz = 0$
all z	$x = 0$	$C_A = C_{A\,bulk}$	$C_B = 0$	$C_C = 0$	$C_D = 0$
all z	$x = 2x_r + x_e$	$dC_A/dx = 0$	$dC_B/dx = 0$	$dC_C/dx = 0$	$dC_D/dx = 0$

Obviously, as C contributes to the overall current in the ECE mechanism, it must be explicitly simulated. As the concentration of A at the electrode surface may be taken as 0 at sufficiently high potentials and is not a function of the concentration of B, it is not necessary to use an iterative method to reach a solution. The solution procedure is therefore to sequentially find A, then B, and then C. D does not need to be simulated to find the current response but, if required, may be found as given.

DISP1 Reaction. In the DISP1 reaction, the formation of A from B necessitates the use of an iterative procedure, and the assumption that the species C is a short-lived intermediate with no appreciable concentration at any point further modifies the above equations to become

$$D\frac{\partial^2 C_A}{\partial x^2} + D\frac{\partial^2 C_A}{\partial z^2} - u\frac{\partial C_A}{\partial x} + k_2 C_B = 0 \quad (18)$$

$$D\frac{\partial^2 C_B}{\partial x^2} + D\frac{\partial^2 C_B}{\partial z^2} - u\frac{\partial C_B}{\partial x} - 2k_2 C_B = 0 \quad (19)$$

$$D\frac{\partial^2 C_D}{\partial x^2} + D\frac{\partial^2 C_D}{\partial z^2} - u\frac{\partial C_D}{\partial x} + k_2 C_B = 0 \quad (20)$$

with the governing equation for species D as in eq 11 and with the following boundary conditions:

$z = 0$	$x < x_r$	$dC_A/dz = 0$	$dC_B/dz = 0$	$dC_D/dz = 0$
$z = 0$	$x_r < x < x_r + x_e$	$C_A = 0$	$dC_B/dz = -dC_A/dz$	$dC_D/dz = 0$
$z = 0$	$x_r + x_e < x$	$dC_A/dz = 0$	$dC_B/dz = 0$	$dC_D/dz = 0$
$z = 2h$	all x	$dC_A/dz = 0$	$dC_B/dz = 0$	$dC_D/dz = 0$
all z	$x = 0$	$C_A = C_{A\,Bulk}$	$C_B = 0$	$C_D = 0$
all z	$x = 2x_r + x_e$	$dC_A/dx = 0$	$dC_B/dx = 0$	$dC_D/dx = 0$

The initial conditions chosen are that $C_B = 0$ at all points, and the concentration of A is determined. The solution procedure is to then find B using the initial distribution of A. These initial values found are then refined by iteration, where new values for A and B are calculated using the values of A and B from the previous iteration in both cases. The values used for the next iteration are then calculated as before by relaxing the values previously used.

DISP2 Reaction. The DISP2 mechanism is formulated similarly to the DISP1 mechanism, except that the rate of the overall reaction is a second-order power of the local concentration of B. As the boundary conditions at the electrode for either DISP process require iteration, the solution procedure is unaffected.

The governing equations are

$$D\frac{\partial^2 C_A}{\partial x^2} + D\frac{\partial^2 C_A}{\partial z^2} - u\frac{\partial C_A}{\partial x} + \frac{k_2 k_4}{k_{-2}} C_B{}^2 = 0 \quad (21)$$

$$D\frac{\partial^2 C_B}{\partial x^2} + D\frac{\partial^2 C_B}{\partial z^2} - u\frac{\partial C_B}{\partial x} - 2\frac{k_2 k_4}{k_{-2}} C_B{}^2 = 0 \quad (22)$$

$$D\frac{\partial^2 C_D}{\partial x^2} + D\frac{\partial^2 C_D}{\partial z^2} - u\frac{\partial C_D}{\partial x} + \frac{k_2 k_4}{k_{-2}} C_B{}^2 = 0 \quad (23)$$

The boundary conditions are as for the DISP1 process, as is the transport equation for D.

CE Reaction. The CE reaction is formulated in a manner similar to the other reactions studied, with the addition of convection in the z direction, which is nonzero over the central region of the cell.

$$D\frac{\partial^2 C_A}{\partial x^2} + D\frac{\partial^2 C_A}{\partial z^2} - u\frac{\partial C_A}{\partial x} - w\frac{\partial C_A}{\partial z} - k_{CE} C_A C_B = 0 \quad (24)$$

$$D\frac{\partial^2 C_B}{\partial x^2} + D\frac{\partial^2 C_B}{\partial z^2} - u\frac{\partial C_B}{\partial x} - w\frac{\partial C_B}{\partial z} - k_{CE} C_A C_B = 0 \quad (25)$$

$$D\frac{\partial^2 C_C}{\partial x^2} + D\frac{\partial^2 C_C}{\partial z^2} - u\frac{\partial C_C}{\partial x} - w\frac{\partial C_C}{\partial z} + k_{CE} C_A C_B = 0 \quad (26)$$

The boundary conditions are

$z = 0$	$x < x_r + x_{be}$	$dC_A/dz = 0$	$dC_B/dz = 0$	$dC_C/dz = 0$
$z = 0$	$x_r + x_{be} < x < x_r + x_{be} + x_e$	$dC_A/dz = 0$	$dC_B/dz = 0$	$C_C = 0$
$z = 0$	$x_r + x_{be} + x_e < x$	$dC_A/dz = 0$	$dC_B/dz = 0$	$dC_C/dz = 0$
$z = h$	$x < x_r$	$dC_A/dz = 0$	$dC_B/dz = 0$	$dC_C/dz = 0$
$z = 2h$	all x	$dC_A/dz = 0$	$dC_B/dz = 0$	$dC_C/dz = 0$
$0 < z < h$	$x = 0$	$C_A = C_{A\,bulk}$	$C_B = 0$	$C_C = 0$
$h < z < 2h$	$x = 0$	$C_A = 0$	$C_B = C_{B\,bulk}$	$C_C = 0$
all z	$x = x_r + x_{be} + x_e + x_{ae}$	$dC_A/dx = 0$	$dC_B/dx = 0$	$dC_C/dx = 0$

Current Calculation. By use of a square interpolation function, for the grid used, the current is given by a sum evaluated over the elements immediately over the electrode

$$I = FDw[C]_{\text{bulk}}\sum_{n=1}^{n_e}\frac{b_j}{2c_k}(C_{n,k} + C_{(n+1),k}) \qquad (27)$$

where $C_{n,k}$ is the concentration at node k of element n.

Results and Discussion

EC Reaction. Compton and Coles[18] showed that the shift of the current−potential curve for an EC reaction is a function of the flow rate and the normalized rate constant

$$K_1 = k_2(h^2 x_e^2/4u_0^2 D)^{1/3} \qquad (28)$$

The effect of the decay of the B species is to reduce the equilibrium concentrations of both A and B at the electrode, as the potential applied fixes the ratio of the A and B concentrations. This reduction of the concentration of the A species at the electrode surface leads to an increase in the current response, compared to that observed where B does not decay. The effect of increasing the rate of decay of B is therefore to shift the potential required to achieve a given current response in the negative direction. The effect of increasing the volume flow rate (Vf), for a constant rate of decay, is to increase both the production of species B, and the speed at which B is transported away from the electrode, resulting in the concentration of B at the electrode remaining closer to that observed in the absence of any decay. As the shape of the current−potential curve remains constant with the variation of K_1, the position of the curve may be characterized by the half-wave potential, at which the current observed is half that found as the potential tends to infinity.

Figure 5 shows the calculated variation of the shift of the half-wave potential, plotted against the log of the normalized rate constant, compared to the values given by Compton et. al. using the BI finite difference method[1], and excellent agreement is noted. The grid parameters used were $n_z = 40$, $n_{xr} = 30$, $n_{xe} = 30$, $z_f = 4 \times 10^{-7}$ cm, $x_{fr} = 4 \times 10^{-6}$ cm, $x_{fe} = 4 \times 10^{-7}$ cm, $h = 0.04$ cm, $x_r = 0.2$ cm, x_e 0.4 cm, $D = 1 \times 10^{-5}$ cm^2 s^{-1}, $w = 0.4$ cm, $d = 0.6$ cm, and Vf = 0.01 cm^3 s^{-1}. The iterative process used re values starting at 0.8 and descending to around 0.2, as the solution converged. The convergence tolerance was set to 1×10^{-3} for all runs, and between 5 and 35 iterations were required for each run to converge, taking 50 s per iteration, on a 100 MHz Pentium, using less than 32 Mb of memory.

ECE and DISP Reactions. For the ECE and DISP reactions, the shift of the current−potential wave for the reduction of A is obscured by the reduction of the C species, and the standard characterization of the process is therefore to examine the variation of the current response at the limiting potential where complete reduction occurs. As the rate of decay of B increases, the effective number of electrons transferred at the electrode for every molecule of A that is reduced, n_{eff}, varies from 1, for

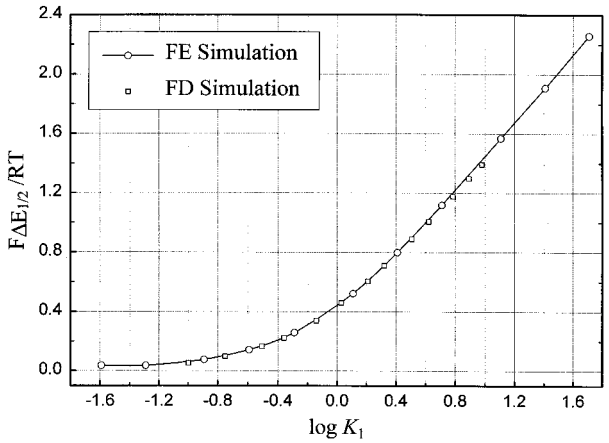

Figure 5. The shift in half-wave potential for an EC reaction.

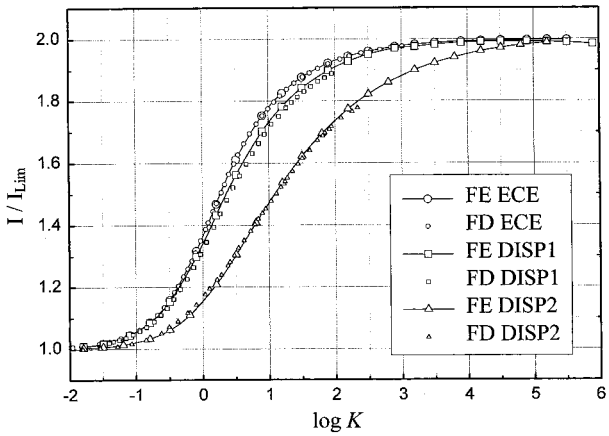

Figure 6. The variation of n_{eff} with the normalized rate constant for ECE, DISP1, and DISP2 reactions.

$k_2 = 0$, to 2, as $k_2 \rightarrow \infty$, in which case the C species is formed within a sufficiently small distance of the electrode to be reduced completely.

The parameter of n_{eff} has been shown to a unique function of K_1 for the ECE or DISP1 mechanisms, or K_2, given below, for the DISP2 mechanism.

$$K_2 = 2(k_2 k_4/k^{-2})C_{\text{bulk}}(h^2 x_e^2/4u_0 D)^{1/3} \qquad (29)$$

Figure 6 shows the calculated values of n_{eff} for the different types of reaction discussed, plotted against the appropriate normalized rate constant. The grid parameters used for the ECE process were $n_z = 40$, $n_{xr} = 30$, $n_{xe} = 30$, $z_f = 5 \times 10^{-7}$ to 2×10^{-8} cm, $x_{fr} = 2 \times 10^{-6}$ cm, $x_{fe} = 2 \times 10^{-6}$ cm, $h = 0.04$ cm, $x_r = 0.2$ cm, x_e 0.4 cm, $D = 1 \times 10^{-5}$ cm^2 s^{-1}, $w = 0.4$ cm, $d = 0.6$ cm, and Vf = 0.01 cm^3 s^{-1}. For the DISP1 and DISP2 reactions, $n_z = 30$, $n_{xr} = 20$, and $n_{xe} = 30$, for DISP1, $z_f = 5 \times 10^{-8}$ cm, and for DISP2, $z_f = 2 \times 10^{-7}$ cm in all cases, and other parameters were as for the ECE reaction. The re values used ranged from 0.8 to 0.08, and around 15−50 iterations were required for almost the whole range of rate constants, rising up to around 100 for the highest rates, each taking around 30 s per iteration on a 100 MHz Pentium with 96 Mb RAM. Convergence tolerances were set between 1×10^{-4} and 1×10^{-5}.

Good agreement between the FE results presented and previous FD work is noted. The FE method is also shown to be capable of handling extremely high rate constants, over 2 orders of magnitude above those previously demonstrated, at a very modest increment in computational time.

CE Reaction using the Confluence Reactor. The confluence reactor geometry was investigated to determine the range of rate constants of a CE reaction that could be distinguished over a practical range of volume flow rates and cell geometries. In this type of experiment, the A and B species are introduced into separate inlets of the reactor and react on mixing to form an electroactive species C, which is reduced at an electrode set into the wall of the cell at a distance downstream.

If the rate of reaction is high enough, however, complete conversion of the A and B species to C will occur. In this case, if the diffusion coefficients of all the species are equal, the concentration of the C species local to the electrode will be identical to the concentration of the B species that would exist in the case where no reaction occurs. This indicates that the cases where a species introduced through the top inlet completely reacts to generate an electroactive species, and the case where the electroactive species itself is introduced through the top inlet, both give rise to the same observed current. The current response in this case may be considered to be the mass transport limited current, I_{lim}, for a particular cell geometry, diffusion coefficient, and volume flow rate.

The variation of I_{lim} is governed by the competition between the rate at which the electroactive species is transported to the electrode by diffusion in the z direction and the rate at which the species is transported past the electrode, and out of the cell, by convection in the x direction. Where the rate at which the solution flows through the cell is low compared to the diffusion coefficient, the concentration of the electroactive species will become uniform in the z direction before the electrode is reached in the x direction. In this case, the current response is identical to that for a channel electrode of the same dimensions, rising in proportion to $\mathrm{Vf}^{1/3}$. As the volume flow rate rises compared to the diffusion coefficient of the electroactive species, the distance downstream in x at which the concentration of the electroactive species becomes uniform in the z direction rises. As this distance exceeds that of the electrode, the current response observed is progressively diminished, as less of the electroactive species is able to diffuse to the electrode before being swept out of the cell.

The resulting current response initially rises with flow rate, in line with the predicted behavior for a channel cell, and then falls off back to zero, at flow rates high enough to prevent the electroactive species diffusing across to the electrode. This has been previously discussed[13] for the case where the electroactive species is introduced into the cell and resembles the hydrodynamic behavior of opposite sided double electrodes.

The limiting currents observed for a range of flow rates and electrode positions are shown in Figure 7 and are found from simulations performed where the B species introduced through the upper inlet is electroactive and no other reactions occur. The geometric parameters used were $n_{za} = 10$, $n_{zb} = 15$, $n_{zc} = 15$, $n_{zd} = 15$, $n_{xr} = 10$, $n_{xbe} = 25$, $n_{xoe} = 20$, $n_{xae} = 10$, $z_{fa} = 2 \times 10^{-3}$ cm, $z_{fb} = 6 \times 10^{-4}$ cm, $z_{fc} = 6 \times 10^{-4}$ cm, $z_{fc} = 2 \times 10^{-5}$ cm, $x_{fr} = 6 \times 10^{-4}$ cm, $x_{fbe} = 6 \times 10^{-4}$ cm, $x_{foe} = 6 \times 10^{-4}$ cm, $x_{fae} = 6 \times 10^{-4}$ cm, $z_a = 0.04$ cm, $z_b = 0.04$ cm, $x_r = 0.4$ cm, $x_e = 0.4$ cm, $x_{ae} = 0.8$ cm, $w = 0.2$ cm, $d = 0.6$ cm, $C_{\mathrm{bulk}} = 0.001$ mol cm^{-3}, $D = 1 \times 10^{-5}$ cm^2 s^{-1}, and x_{be} varies as indicated.

The linear increase with $\mathrm{Vf}^{1/3}$ at low flow rates demonstrates that complete conversion to the C species is occurring before the electrode. This persists up to higher volume flow rates to an extent that is dependent on how far the electrode is from the union of the two inlets. It must be noted that due to the height of the confluence reactor, at the slower flow rates used, the Lévêque approximation begins to fail. For the lowest flow rates, the parameter $2\mathrm{Vf}h/D\ \mathrm{d}x_e = 1.33$, whereas for the Lévêque approximation and the Levich equation to be accurate, this parameter must be far in excess of unity. The limiting currents over the linear portion of Figure 7 are therefore lower than those predicted by the Levich equation.

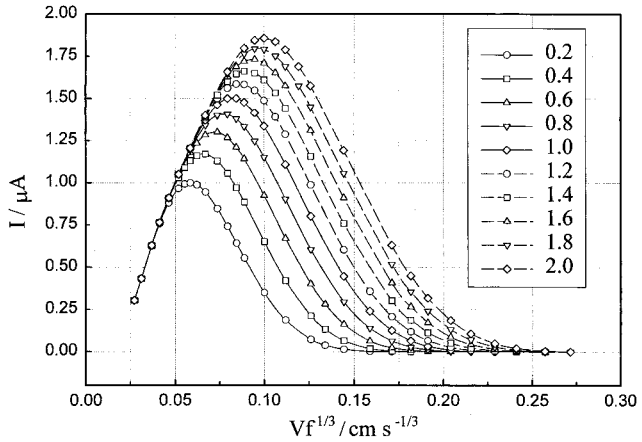

Figure 7. Limiting currents observed at the confluence reactor, for values of x_{be} indicated in cm.

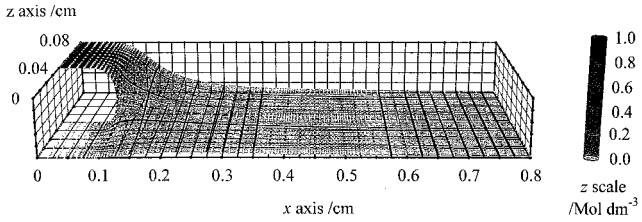

Figure 8. B concentration profile at $\mathrm{Vf} = 5 \times 10^{-5}$ cm^3 s^{-1}, with $k_{\mathrm{CE}} = 50$ mol^{-1}dm^3 s^{-1}.

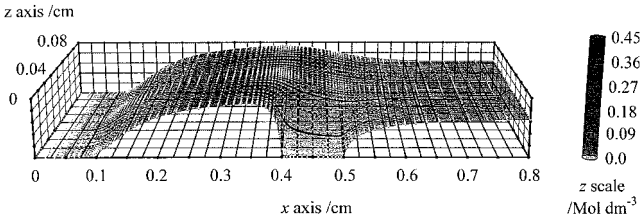

Figure 9. C concentration profile at $\mathrm{Vf} = 5 \times 10^{-5}$ cm^3 s^{-1}, with $k_{\mathrm{CE}} = 50$ mol^{-1}dm^{3}s^{-1}.

The behavior of the confluence reactor when examining the CE reaction may be better visualized by considering concentration profiles showing the distributions of the reactant and product species throughout the region of interest. Figure 8 shows the concentration profile of the B species, entering through the upper inlet in a confluence reactor, for the parameters given below. In this case, the rate of reaction is fast compared to the flow rate, and the B species is destroyed almost completely within a few millimeters of the union of the inlets.

For the purposes of clear illustration, these grids contain significantly fewer nodes, shown as white spheres, and larger minimum node spacings than were used otherwise. The main geometric parameters used were $z_a = 0.04$ cm, $z_b = 0.04$ cm, $x_r = 0.1$ cm, $x_{be} = 0.3$ cm, $x_e = 0.1$ cm, $x_{ae} = 0.3$ cm, and $C_{\mathrm{bulk}} = 0.001$ mol cm^{-3} for A and B, and $D = 1 \times 10^{-5}$ cm^2 s^{-1}, for all species. As, under these conditions, the concentrations of the A and B species are completely symmetrical in y, only the B and C species need be shown.

Figure 9 shows the corresponding concentration profile of C. It can be observed that almost complete conversion of A

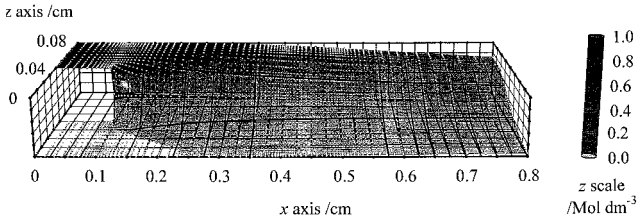

Figure 10. B concentration profile at $Vf = 1 \times 10^{-3}$ cm^3 s^{-1}, with $k_{CE} = 50$ mol^{-1}dm^{3}s^{-1}.

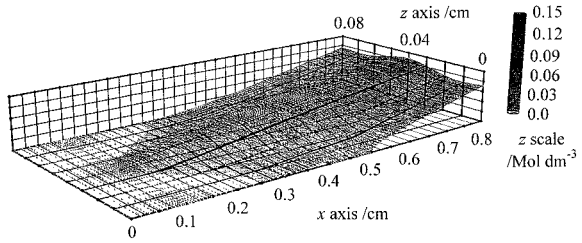

Figure 11. C concentration profile at $Vf = 1 \times 10^{-3}$ cm^3 s^{-1}, with $k_{CE} = 50$ mol^{-1}dm^{3}s^{-1}.

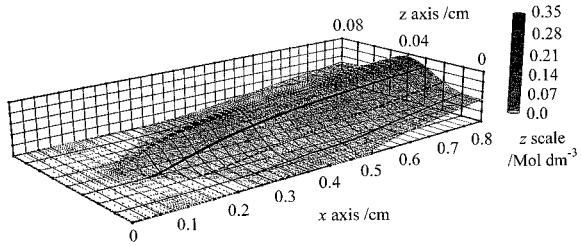

Figure 12. C concentration profile at $Vf = 1 \times 10^{-3}$ cm^3 s^{-1}, with $k_{CE} = 500$ mol^{-1}dm^{3}s^{-1}.

and B to C occurs before the electrode, bearing in mind that full conversion would yield C concentrations of 0.5, not 1.0, relative to the bulk values of A and B. Increasing the rate of reaction in this case would therefore have little effect. In addition, the concentration of the C species approaching the electrode is very uniform in *y*, which is the criterion for channel cell-like behavior.

Figures 10 and 11 show the case where the flow rate is sufficiently high that only a negligible proportion of the B and C species can diffuse to the electrode. The A and B species do not become uniformly distributed until far beyond the electrode, and consequently, the C species is generated mainly at the center of the cell in *y* and cannot diffuse to the electrode before being swept downstream.

Figure 12 shows the effect on the C species of increasing the rate of reaction. Although more of the C species is generated, the fraction that is able to diffuse to the electrode is still very small. As the transport limited current for this flow rate is also very small, for this CE reaction, the ratio of the current observed from the reduction of C to the transport limited current is 0.94, confirming that increasing the rate of reaction further does not increase the current appreciably. This compares to $I/I_{lim} = 0.52$ in the previous example.

The rate of the reaction between A and B may be seen to determine the variation of the current observed between zero, where there is no reaction, and I_{lim} at sufficiently high reaction rates. It has been found that where diffusion coefficients are homogeneous, a unique surface exists for the variation of I/I_{lim} against dimensionless $k_{CE}h^2C_{bulk}/D$ and Vfh/Dx_c in centimeters, where $x_c = x_{be} + 0.625x_e$. This surface is shown in Figure 13, generated using the same parameters as for Figure 7, except for $x_{ae} = 0.75$ cm.

The plot shown in Figure 13 allows the current response for the CE reaction to be determined in relation to I_{lim}. The usefulness of this is that I_{lim} can be determined experimentally by introducing the electroactive species through the upper inlet. Provided that the diffusion coefficient is the same, it is not even necessary for an identical species to be used. Therefore, the results of experiments using the confluence reactor may be used to determine the rate constant for a CE reaction using the surface in Figure 13, without recourse to any further simulation. It is also evident that the curves presented in Figure 13 remain invariant with changes in the rate of reaction if C_{bulk} is also varied so as to keep $k_{CE}C_{bulk}$ constant, extending the potential experimental flexibility of this novel cell.

Conclusion

The results presented indicate that the finite element method is a useful tool to investigate the behavior of systems where coupled kinetic processes play a role, particularly where the rates of reaction are very fast, and fleeting intermediates are encountered.

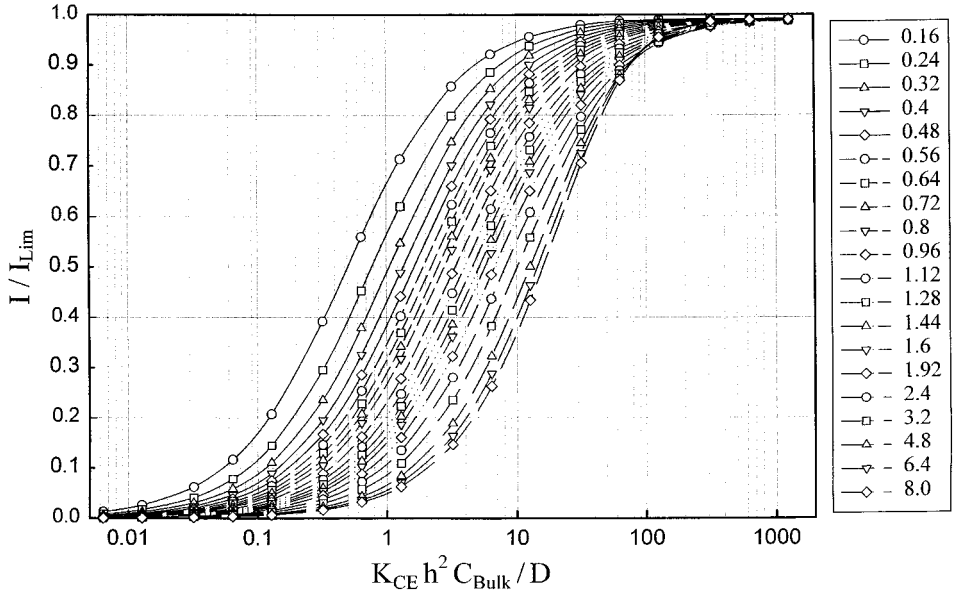

Figure 13. Plot of I/I_{lim} against $k_{CE}h^2C_{bulk}/D$ for indicated values of Vfh/Dx_c.

The confluence reactor is shown to hold great potential for investigating reactions where the first step involves a homogeneous reaction. The ease with which different parameters may be adjusted to study a wide range of reaction rates, particularly fast reactions that could not be so easily tackled using other geometries, commend this new cell to the experimentalist. Future work will seek to rationalize the behavior encountered where inhomogeneous diffusion coefficients are found, and further extend the practical application of this cell geometry.

Acknowledgment. We thank the U.K. EPSRC for Ph.D. Studentship 957 00 361 and the U.K. Royal Society of Chemistry for postdoctoral support for N.S.

References and Notes

(1) Compton, R. G.; Pilkington, M. B. G.; Stearn, G. M. *J. Chem. Soc.* **1988**, *84* (6), 2155−2171.

(2) Coles, B. A.; Dryfe, R. A. W.; Rees, N. V.; Compton, R. G.; Davies, S. G.; McCarthy, T. D. *J. Electroanal. Chem.* **1996**, *411*, 121−128.

(3) Alden, J. A.; Feldman, M. A.; Hill, E.; Prieto, F.; Oyama, M.; Coles, B. A.; Compton, R. G. *Anal. Chem.* **1998**, *70*, 1707−1720.

(4) Alden, J. A.; Compton, R. G. *J. Phys. Chem. B.* **1997**, *101*, 8941−8954.

(5) Prieto, F.; Aixill, W. J.; Alden, J. A.; Coles, B. A.; Compton, R. G. *J. Phys. Chem. B.* **1997**, *101*, 5540−5544.

(6) Alden, J. A.; Compton, R. G. *J. Phys. Chem. B* **1997**, *101*, 9606−9616.

(7) Prieto, F.; Webster, R. D.; Alden, J. A.; Aixill, W. J.; Waller, G. A.; Compton, R. G.; Rueda, M *J. Electroanal. Chem.* **1997**, *437*, 183−189.

(8) Engblom, S. O.; Myland, J. C.; Oldham, K. B. *Anal. Chem.* **1994**, *66*, 3182−3187.

(9) Aixill, W. J.; Alden, J. A.; Prieto, F.; Waller, G. A.; Compton, R. G.; Rueda, M. *J. Phys. Chem. B* **1998**, *102*, 1515−1521.

(10) Alden, J. A.; Compton, R. G.; Dryfe, R. A. W. *J. Electroanal. Chem.* **1995**, *397*, 11−17.

(11) Feldberg, S. W.; Goldstein, C. I.; Rudolph, M. *J. Electroanal. Chem.* **1996**, *413*, 25−36.

(12) Stevens, N. P. C.; Fisher, A. C. *J. Phys. Chem. B* **1997**, *101*, 8259−8263.

(13) Fulian, Q.; Stevens, N. P. C.; Fisher, A. C. *J. Phys. Chem. B* **1998**, *102*, 3779−3783.

(14) Stevens, N. P. C.; Fisher, A. C. *J. Phys. Chem. B* **1997**, *101*, 8259−8263.

(15) Stevens, N. P. C.; Hickey, S. J.; Fisher, A. C. *An. Quim.* **1997**, *93*, 225−232.

(16) Rao, S. S. *The Finite Element Method in Engineering*; Pergamon Press: Oxford, 1982.

(17) Cuvelier, C.; Segal, A.; Steenhoven, A. A. *Finite Element Methods and Navier−Stokes Equations;* D. Reidel Publishing Co.: Dordrecht, Holland, 1986.

(18) Coles, B. A.; Compton, R. G. *J. Chem. Soc., Faraday Trans. 1* **1988**, *84* (6), 2155−2171.